requency Waves and Traveling Storm Tracks. Part II: Three-Dimensional Structure

MING CAI AND HUUG M. VAN DEN DOOL

Cooperative Institute for Climate Studies, Department of Meteorology, University of Maryland, College Park, Maryland

(Manuscript received 1 August 1991, in final form 20 March 1992)

ABSTRACT

A special composite technique ("phase shifting" method) that records both the low- and high-frequency transient activity throughout the troposphere in a framework moving with an individual low-frequency wave of 500-mb geopotential height at 50°N was used to document the three-dimensional structure of the planetary-scale low-frequency waves as well as the attendant traveling storm tracks from the NMC twice-daily analyses of geopotential height and temperature at pressure levels 850, 700, 500, 300, and 200 mb for the ten winters 1967/68 through 1976/77.

The following are the main characteristics of the Northern Hemisphere midlatitude planetary-scale low-frequency waves (zonal wavenumber $m = 1, 2, 3$, and 4) in winter: (i) The amplitude of the planetary scale low-frequency waves is nearly constant with the zonal wavenumber m, and has a maximum at 300 mb for geopotential height and at 850 mb for temperature; (ii) All low-frequency waves have a nearly equivalent barotropic structure (much more so than the stationary waves); (iii) The instantaneous zonal phase speed of an individual low-frequency wave is nearly independent of height and latitude so that we may identify the three-dimensional structure of a low-frequency wave by following that wave at just one pressure level and one latitude in either geopotential height or temperature.

The traveling storm tracks, defined as the local maxima on the rms map of the phase-shifted high-frequency eddies, are identifiable from both geopotential height and temperature data throughout the troposphere. They are located over the trough regions of the low-frequency waves. The barotropic feedback (i.e., the geopotential tendency due to the vorticity flux) of the traveling storm tracks tends to reinforce the low-frequency waves and to retard their propagation throughout the troposphere. The baroclinic feedback (i.e., the temperature tendency due to the heat flux) of the traveling storm tracks appears to have an out-of-phase relation with the low-frequency waves in temperature from 850 mb to 300 mb. At 200 mb, the baroclinic feedback is nearly in phase with the low-frequency waves in the temperature field.

The mutual dependence between the low-frequency flow and their attendant traveling storm tracks dynamically resembles that between the climatological stationary waves and the climatological storm tracks. Therefore, our observational study seems to lend support for the local instability theory that accounts for the existence of the stationary/traveling storm tracks as the consequence of the zonal inhomogeneity of the climatological mean/low-frequency flow.

1. Introduction

In Cai and Van den Dool (1991; hereafter referred to as Part I), we have documented the existence of traveling storm tracks as well as their spatially coherent relation to the low-frequency waves with ten-year winter data of 500-mb geopotential height over the Northern Hemisphere. The symbiotic relation between the low-frequency waves and the traveling storm tracks was described with a then-novel diagnostic technique ("phase shifting" method) that records the high-frequency activity in a framework moving with an individual low-frequency planetary-scale wave. The low-frequency planetary-scale waves organize the high-frequency eddies such that the latter tend to preferentially intensify over the trough regions of the former, giving rise to the storm tracks that travel along with a speed not very different from that of the low-frequency waves. The vorticity flux associated with the traveling storm tracks tends both to reinforce the low-frequency waves and to retard their propagation. The barotropic component of this relation between the low-frequency flow and the traveling storm tracks is dynamically equivalent to that between the climatological stationary waves and the climatological storm tracks, which has been documented intensively in the literature (e.g., Blackmon et al. 1977; Lau and Holopainen 1984).

Part I is based on the analysis of the geopotential height data at 500 mb only. We now report an extended analysis made with a multilevel dataset and including temperature. As in Part I, the phase-shifting method is our primary tool for the analysis. One of our objectives is to identify the three-dimensional structure of the low-frequency waves themselves. To our knowledge, no study has systematically and explicitly doc-

Corresponding author address: Dr. Ming Cai, University of Maryland, Department of Meteorology, 2213 Computer & Space Science Building, College Park, MD 20742.

umented the three-dimensional structure of the low-frequency waves (one may indirectly deduce the structure of the low-frequency waves from an extended Eliassen–Palm flux analysis as in Hoskins et al. 1983). We also wish to document the three-dimensional structure of both barotropic and baroclinic low-frequency tendency fields induced by the high-frequency eddies.

As shown in the observational study of Lau and Holopainen (1984) and the theoretical/modeling study of Cai and Mak (1990a), the high-frequency transients organized by a zonally asymmetric stationary jet stream have a positive (negative) feedback effect upon the barotropic (baroclinic) component of the jet stream. This dual-feedback effect of the high-frequency eddies upon the low-frequency flow has also been found in many case studies of blocking episodes (see references in Part I for a review of the literature on this subject). Such dual-feedback effect is found to be the key mechanism that couples planetary-scale waves with synoptic-scale waves (Cai and Mak 1990b). The barotropic component of the optimal coupling between low-frequency flow patterns and high-frequency eddies has also been systematically studied in the publications of Metz with a fairly new analysis tool, namely, canonical correlation analysis (Metz 1989, 1990, 1991). In a recent observational study, Lau and Nath (1991) found that the month-to-month variability of the (quasi-stationary) storm tracks is coupled to the anomaly of the monthly mean large-scale circulation. The barotropic (baroclinic) feedback associated with the monthly variability of the storm tracks appears to have a positive (negative) spatial correlation with the monthly geopotential height (temperature) anomaly. Therefore, our efforts to document the relationship between low-frequency waves and traveling storm tracks would be incomplete without including baroclinic feedback effect of the high-frequency eddies associated with the traveling storm tracks.

Our general approach to the problem of mutual dependence of the low- and high-frequency fluctuations is different from that employed in Lau and Nath (1991). They first determined the principal month-to-month fluctuation modes from the monthly rms maps of the high-frequency eddies. The coupling mechanism between low- and high-frequency fluctuations was then examined by identifying the joint month-to-month variability in the geopotential height field and the (baroclinic and barotropic) feedbacks associated with the monthly rms modes of the high-frequency eddies. Therefore, the low-frequency phenomena studied in Lau and Nath (1991) are limited to those with time scales of a month or longer. Moreover, their low-frequency phenomena are mostly related to the well-known PNA, EA, and WA teleconnection patterns, which have a spatially fixed, nonmoving structure. The relationship of the low-frequency flow and the high-frequency eddies, however, is not particularly related or limited to just teleconnection patterns or to the extreme blocking cases. We here attempt to study, in general terms, how low-frequency phenomena with a time scale from a week to a season relate to high-frequency eddies with filtered data which are available on a day-to-day basis. Low-frequency patterns with such a broad spectrum of time scale are expected to be both mobile and "standing" and are not constrained to be teleconnection patterns or blockings.

The outline of this article is as follows. In the next section we describe the dataset used in this study and the method of analyses. A brief description of the wintertime climatology of the Northern Hemispheric midlatitude circulation is given in section 3, emphasizing the baroclinic component and the vertical structure of the high-frequency feedbacks upon the stationary waves. Together with section 3 in Part I, this section serves mostly as a reference for the documentation of the symbiotic relation between the low-frequency waves and the high-frequency eddies. Section 4 reports the results showing the traveling storm tracks deduced from the temperature field associated with each of the first four low-frequency waves as well as their baroclinic feedbacks upon the low-frequency waves. The vertical structure of the low-frequency waves and the feedback fields of the high-frequency eddies are presented in section 5. Some theoretical implications of this observational study are discussed in the final section.

2. Data and methods

a. Data

The dataset used in this study consists of the NMC twice-daily analyses of geopotential height and temperature at pressure levels 850, 700, 500, 300, and 200 mb for the ten winters 1967/68 through 1976/77. The winter season is taken to be the 90-day period starting on 1 December. The data are stored on a $4° \times 5°$ latitude–longitude grid covering the area from 22°N to the North Pole. Therefore, we have 72 grid points in the zonal direction and 18 grid points in the meridional direction. Readers are referred to Part I for more details and references of this dataset.

b. Filtering technique

As in Part I, a time spectral (Fourier) decomposition technique has been used to separate the low-frequency from the high-frequency eddies. In our working definition, the low-frequency flow consists of the fluctuations with periods between a week and a season while the high-frequency transient consists of the fluctuations with periods less than a week. The spectral filtering was applied independently to height and temperature at all five levels to a segment of 90 days. Note that, in doing so, the fluctuations on interannual time scales are not included. Of course, the spectral decomposition method is not a perfect filter technique since the time

series is by no means periodic. A filtering technique such as employed by Blackmon (1976) has better characteristics in this regard. In addition, our (or any other) definition of high- and low-frequency fluctuations is somewhat arbitrary. However, with broadband resolution sought, a spectral technique should be adequate to distinguish the fluctuations in high and low frequencies. As shown in Part I, the variance maps of the transients obtained with our spectral technique have the same characteristics as those of other studies in spite of differences in the filtering technique and the precise definitions of the high- and low-frequency fluctuations.

In addition to the time filtering, we shall also decompose the field into a zonal mean and a wave portion. The wave components of a particular flow are obtained by performing a Fourier analysis in the zonal direction according to Eq. (2) in Part I.

c. Feedback analysis

In this study, the tendencies induced by the vorticity and heat fluxes associated with the high-frequency eddies are calculated according to

$$\chi^Z \equiv \left(\frac{\partial Z}{\partial t}\right) = \nabla^{-2}\left(-\frac{f_0}{g}\nabla\cdot(\mathbf{v}'\zeta')\right), \quad (1a)$$

$$\chi^T \equiv \left(\frac{\partial T}{\partial t}\right) = -\nabla\cdot(\mathbf{v}'T'). \quad (1b)$$

We also refer to χ^Z and χ^T as the barotropic and baroclinic feedbacks of the high-frequency transients, respectively. In (1), $\mathbf{v}'$ and ζ' are the geostrophic wind and vorticity of the high-frequency transients, g is the gravity, and f_0 is the Coriolis parameter at 45° latitude. Equation (1) is a method of evaluating the impact of eddies. The total tendencies in Z and T are due to many other terms, which will be discussed in section 6d. It should be noted that χ^Z (or χ^T) does not include effects of the so-called secondary circulation generated by the heat (or vorticity) flux of the transients, which can be incorporated by solving a quasigeostrophic potential vorticity equation (Lau and Holopainen 1984). However, this would require a vertical boundary condition for the transients. As pointed out in Lau and Holopainen (1984), there are some uncertainties in defining the vertical boundary condition for just the transients. Moreover, observational studies have shown that the tendencies induced by the transients are primarily determined by the convergence of the eddy vorticity and heat fluxes, whereas the secondary circulation only plays a minor role (e.g., Pfeffer 1981; Lau and Holopainen 1984; Pierrehumbert 1986; Lau and Nath 1991). We may also add here that relative to the primitive equations, (1b) is exact and so is (1a) except that the streamfunction is replaced by geopotential. We therefore decided that Eq. (1) is a satisfactory first approximation. We shall come back to this issue in section 6a.

We solve (1) by replacing the horizontal derivatives with the centered finite-difference formulas. As in Part I, we shall only evaluate the wave portion of χ^Z and χ^T at each level (for the sake of brevity, we shall still use the symbols χ^Z and χ^T to denote the *wave portion* of χ^Z and χ^T). Obviously, we do not need any boundary conditions to obtain a solution to (1b). The boundary condition for χ^Z at 90°N is $\chi^Z = 0$ since there is no wave at the pole. The boundary condition for χ^Z at 22°N is artificially assumed to be $\partial\chi^Z/\partial\phi = 0$. It has been tested that the solutions for χ^Z over most of the area poleward from 22°N are not sensitive to the particular boundary conditions except in the vicinity of the boundary.

We have calculated the tendency fields χ^Z and χ^T at each observation time. The time mean of χ^Z and χ^T gives rise to the feedbacks of the high-frequency transients to the climatological stationary waves. The low-frequency component of the tendency fields induced by the high-frequency eddies is defined as the feedback of the high-frequency eddies to the low-frequency fluctuations.

d. Phase-shifting method

In Part I, we have used the phase-shifting technique to identify the time-mean structure of the low-frequency waves as well as their attendant traveling storm tracks at 500 mb. The phase-shifting technique is a special composite analysis that follows an individual low-frequency wave in a frame moving with a speed equal to the instantaneous phase speed of the low-frequency wave at reference latitude, ϕ_0. In such a moving frame, the traveling planetary-scale wave becomes stationary and so are its attendant storm tracks (if any). Hence, we may deduce the time-mean structure of the low-frequency waves and the traveling storm tracks as well as the feedback effects of the traveling storm tracks upon the low-frequency waves from the statistics calculated in the moving frame. In Part I, we have demonstrated that the zonal inhomogeneity in the statistics of the phase-shifted flow is practically free from that calculated in the stationary frame (there is no mathematical proof that this ought to be so). Thus, the phase-shifting technique is capable of separating the traveling planetary-scale waves and the traveling storm tracks from the stationary ones. Intuitively, this is explainable from the fact that the moving frame has little preference for residing in any longitude sector (cf. Fig. 10 in Part I).

In Part I, we only needed to be concerned with preserving the meridional structure of the phase-shifted flow since our analysis was made with only one-level data. We present here a generalized version of the phase-shifting formula that includes a reference pressure level p_0 as well because the preservation of the

vertical structure of the phase-shifted flow is an issue now. Let $\hat{\xi}(\lambda, \phi, p, t)$ be the phase-shifted flow constructed from the original flow $\xi(\lambda, \phi, p, t)$, where ξ can be geopotential height, temperature, or any observed/derived variables. The phase-shifting formula for our multilevel data analysis is

$$\hat{\xi}(\lambda, \phi, p, t) = \xi(\lambda - \lambda^*(t; \phi_0, p_0, \text{other reference parameters}), \phi, p, t), \quad (2)$$

where $\lambda^*(t; \phi_0, p_0,$ other parameters) is a function of time only and measures the phase angle by which the map $\xi(\lambda, \phi, p, t)$ has to be longitudinally shifted at time t to become $\hat{\xi}(\lambda, \phi, p, t)$. In (2), ϕ_0 and p_0 are the reference latitude and pressure, respectively. The other reference parameters, such as the reference variable, reference pattern, and reference time, also enter the choice of λ^*. The reference variable and pattern together with the reference latitude and pressure determine the target to be followed in the process of transforming the map $\xi(\lambda, \phi, p, t)$ to the map $\hat{\xi}(\lambda, \phi, p, t)$. The reference time gives us a choice of the lagged, simultaneous, or lead phase shifting relative to the target.

For an easy comparison of the results reported here to those in Part I, we shall use the same reference parameters for our multilevel data analysis. Specifically, the reference variable is the low-frequency component of geopotential height. We have four reference patterns to be followed. They are the low-frequency waves m_0 with $m_0 = 1$, 2, 3, and 4 of the geopotential height at the reference latitude $\phi_0 = 50°$N and at the reference pressure level $p_0 = 500$ mb and at time t (a simultaneous phase shifting). As in Part I, the new longitude of the ridge of a wave m_0 of the phase-shifted low-frequency geopotential height at the reference latitude and pressure level has been taken arbitrarily but intentionally to be the longitude of its counterpart stationary wave m_0. This allows easy comparison of the time-mean structure of the traveling low-frequency waves as well as the attendant rms statistics to their stationary counterparts. A randomizer $\mathcal{R}_{m_0}(t)$ is again used here to select randomly the m_0 possible positions for the low-frequency wave m_0 with an equal probability.[1] The time series of $\mathcal{R}_{m_0}(t)$ used in this paper is identical to that used in Part I. Hence, the *same* moving frame for a wave m_0 ($m_0 = 1$, 2, 3, and 4) used in Part I will be employed here to calculate the statistics of the phase-shifted geopotential height and temperature fields at all levels. A series of experiments indicates that the meridional and vertical structure of the phase-shifted flow is not very sensitive to the choice of ϕ_0 and p_0 as well as the choice of the reference variable. A lagged (or lead) phase shifting enables us to study the propagation of the low-frequency waves as well as their relation to the feedback of the high-frequency eddies a few days earlier (or later). It is found that the results obtained with a lagged (or lead) phase shifting ($\tau < 5$ days) exhibit a nearly identical wave pattern to those reported in sections 4–5 ($\tau = 0$) except for a small shift of the trough and ridge positions, indicating the propagation of the waves.

[1] Without this randomizer, the moving frame with $m_0 \geq 2$ would cover only a part of the latitude circle since $0 \leq \lambda^* \leq 2\pi/m_0$. This implies that the phase-shifting method would lose its effectiveness for a large value of m_0 and thereby would fail to remove the stationary signal. With inclusion of this randomizer, the moving frame for a given m_0 can cover the whole latitude circle, which in particular implies that the range of the moving frame now is no longer a function of m_0.

3. Stationary waves and eddy-induced forcing

The climatology of the stationary waves and the transients as well as the eddy-induced forcing has been well documented in the literature (e.g., Blackmon et al. 1977; Wallace 1983; Wallace and Blackmon 1983; Lau and Holopainen 1984). In section 3 of Part I, we have shown some wintertime statistics of the 500-mb geopotential height as reference to the main theme of the study, namely, the symbiotic relation between low-frequency waves and the traveling storm tracks. We wish to present here some additional material of the climatological wintertime statistics of the midlatitude general circulation that is not quite readily available in the literature. The emphasis here is on the vertical structure of the geopotential height and temperature stationary waves as well as the eddy-induced feedback fields. It should be reminded that none of the results presented in this section has anything to do with the phase-shifting procedure.

The stationary storm tracks (local maxima on the high-frequency rms map) are identifiable from both geopotential height and temperature data. The local maxima on the high-frequency rms maps are placed downstream of the major troughs of the stationary waves. The only exception is the high-frequency rms map of the 850-mb temperature, which exhibits local maxima over the continents instead of over the east coasts of the continents. The signals of the storm tracks in the temperature field are more evident at lower levels, whereas the intensity of the storm tracks in the height field is strongest at the tropopause.

In order to gain more insight into the relation between the stationary waves and the stationary storm tracks, it is instructive to examine both the barotropic and baroclinic feedback effects of the high-frequency eddies on the stationary waves. Plotted in Fig. 1 are the vertical cross-section diagrams along 50°N of stationary waves in both geopotential height and temperature fields [panels (a) and (b)] and the height and temperature feedbacks [i.e., χ^Z and χ^T defined in Eq. (1)] of the high-frequency eddies [panels (c) and (d)]. It is seen that the stationary waves are dominated by wavenumbers 1 and 2. The baroclinic character of the

stationary waves is recognizable from the vertical tilt of troughs and ridges. The time mean of the height tendency χ^Z induced by the vorticity flux of the high-frequency eddies (denoted as χ^Z) clearly plays a forcing role to the stationary waves in Z. The χ^Z field reaches its maximum near the tropopause where the amplitude of the stationary waves in the height field is also the largest. Unlike the stationary waves, the troughs and ridges of the χ^Z field appear to have little tilt with height. The temperature tendency χ^T induced by the heat flux of the high-frequency eddies tends to diminish the stationary waves in T. The maximum of χ^T is found near the surface where the amplitude of the stationary waves in the temperature field also reaches its maximum. Note that the in-phase relation between $\bar{Z}^W$ (the overbar denotes the wintertime mean and the superscript "W" stands for the wave portion of the flow) and χ^Z is almost perfect everywhere. In contrast, the out-of-phase relation between $\bar{T}^W$ and χ^T holds only approximately with several notable exceptions, for instance, at 200 mb where $\bar{T}^W$ is more or less in phase with χ^T.

Figure 2 shows how the time-mean amplitude of the stationary, low-frequency, and high-frequency waves in geopotential height vary as a function of pressure and zonal wavenumber at latitude 50°N. This supplements the information shown in Fig. 2 of Part I. The amplitude of the stationary waves (upper panel) decreases very sharply as the wavenumber increases. We also see that the amplitude of the planetary-scale stationary waves ($m \leq 3$) increases with height, whereas that of the shorter stationary waves ($m > 3$) is practically constant throughout the troposphere. In contrast to the stationary waves, the low-frequency waves (middle panel) have a relatively flat spectrum at the longer wave range ($m \leq 4$). Beyond $m = 4$, the amplitude decreases gradually as the wavenumber increases. An important feature is that the amplitude of the low-frequency waves is comparable to that of the stationary waves. The vertical variation of the amplitude of the longer low-frequency waves is much stronger than that of the shorter low-frequency waves. All low-frequency waves have the largest amplitude at 300 mb. Zonal wavenumber 6 has the largest amplitude among the high-frequency waves (lower panel). The amplitude of the high-frequency waves also has its maximum at 300 mb. For easy comparison, the contour interval in the middle and bottom panels is the same, bringing out that the high-frequency disturbance is only half as strong as the low-frequency disturbance.

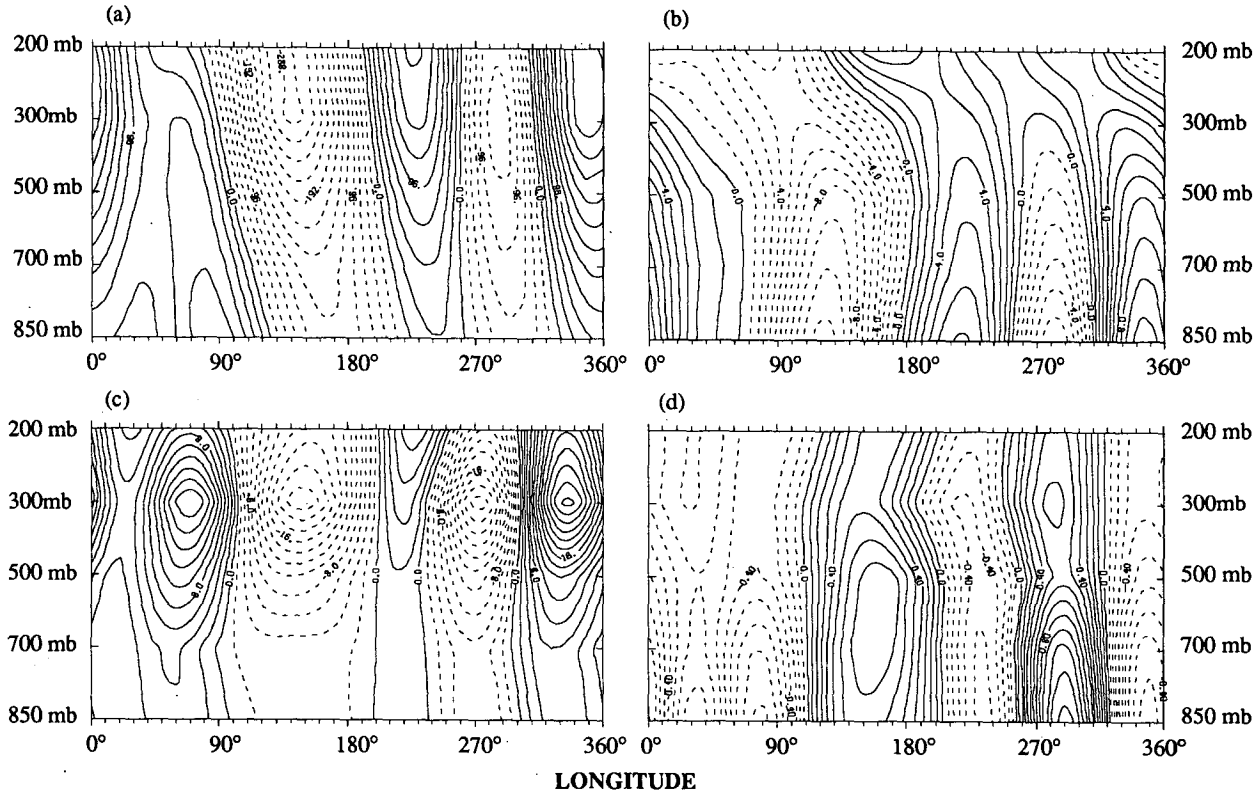

FIG. 1. Vertical cross-section diagrams along the latitude 50°N. (a) Stationary waves in the geopotential height field. (b) Stationary waves in the temperature field. (c) The geopotential height tendency induced by the vorticity flux of the high-frequency eddies. (d) The temperature tendency induced by the heat flux of the high-frequency eddies. The contour intervals for panels (a), (b), (c), and (d) are 24.0 m, 1.0°C, 2.0×10^{-5} m s^{-1}, and 0.1×10^{-5} °C s^{-1}, respectively.

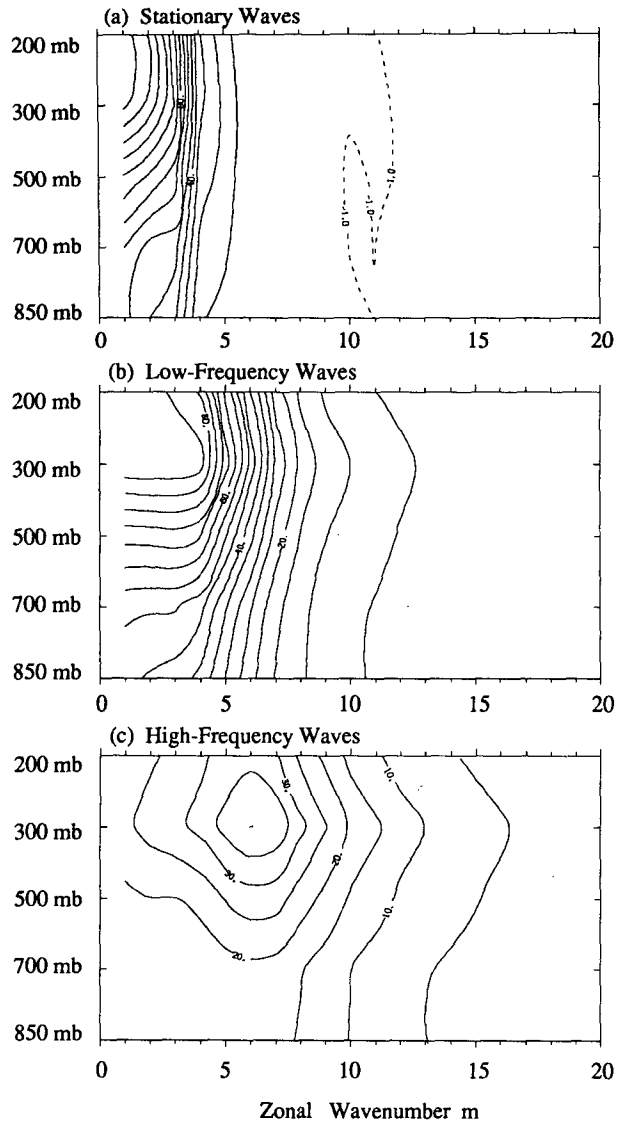

FIG. 2. The time-mean amplitude of (a) the stationary waves, (b) the low-frequency waves, and (c) the high-frequency waves of the geopotential height at latitude 50°N as a function of the zonal wavenumber and pressure. The contour interval for panel (a) is 10 m and that for panels (b) and (c) is 5 m.

Going from top to bottom panels, one can see that the maximum amplitude shifts from low to high zonal wavenumbers as frequency increases.

Figure 3 is identical to Fig. 2 except for temperature. The contour interval is 0.2°C for both low- (middle panel) and high-frequency (bottom panel) disturbances but that for the stationary waves (top panel) is 0.5°C. The stationary waves in temperature are much stronger than the temperature transients. It is also seen that the amplitude of the temperature waves in all three panels exhibits its maximum value near the ground instead of near the tropopause as the case for the height. An outstanding feature in the spectrum of the stationary waves is that wavenumber 2 is very strong (6.5°C) at 850 mb, which obviously results from the land–ocean contrast. At the upper level, the dominant wave in the stationary temperature waves is $m = 1$. The vertical variation of the amplitude of stationary T is generally weak throughout the vertical column except $m = 2$ near the lower boundary, where it decreases with height abruptly. The amplitude of the temperature (high- and low-frequency) transients is almost constant with height at the lower levels and varies more strongly near the tropopause. The minimum amplitude of the temperature transients is placed near 300 mb. The wavenumber 1 is the strongest low-frequency wave, whereas

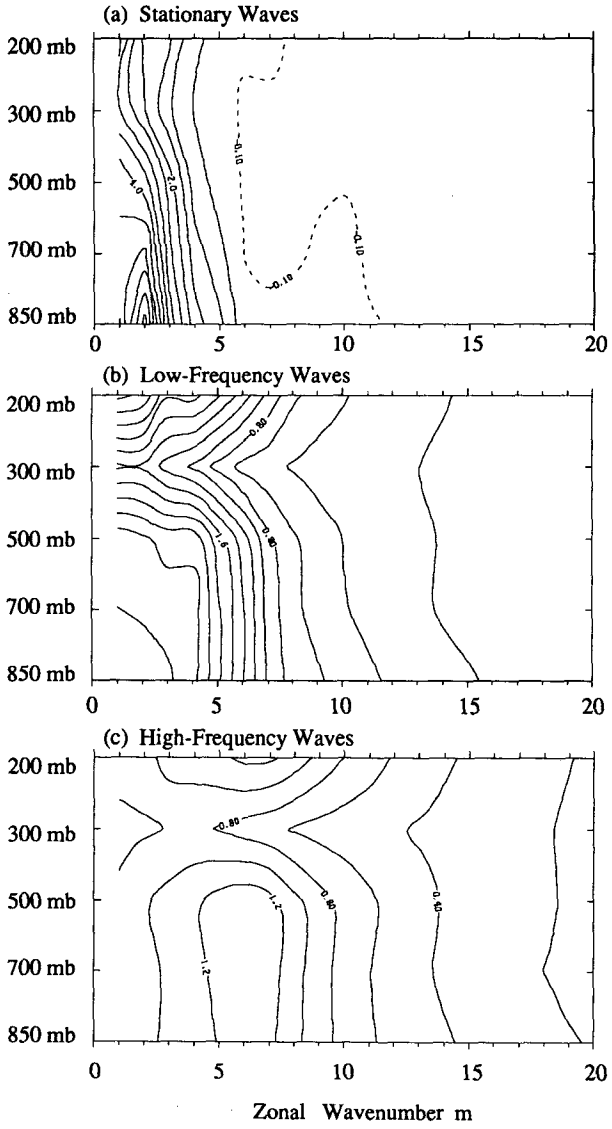

FIG. 3. As in Fig. 2 except for the temperature. The contour interval for panel (a) is 0.5°C and that for panels (b) and (c) is 0.2°C.

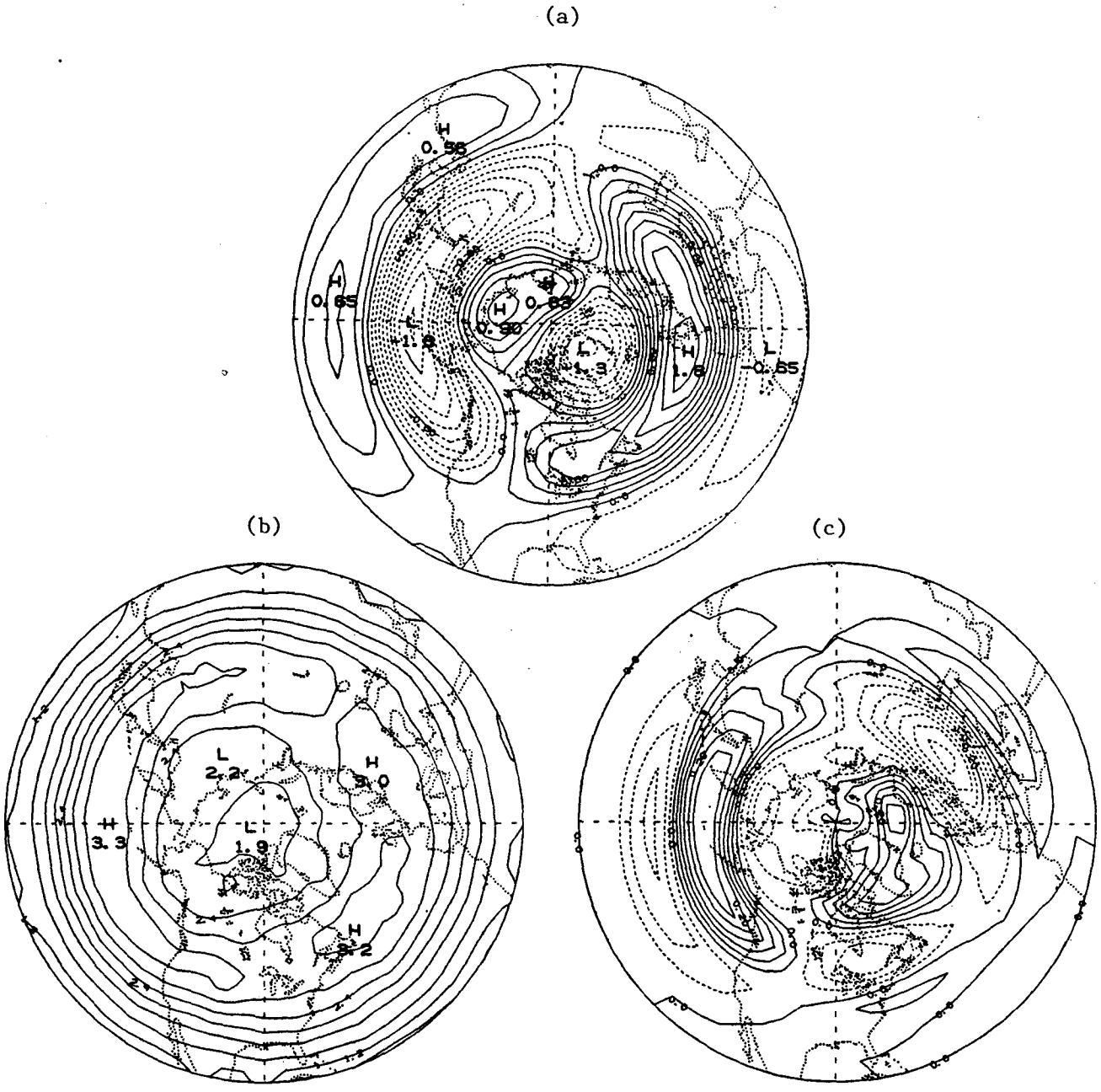

FIG. 4. Statistics of the phase-shifted flow of the 700-mb temperature with $m_0 = 1$. (a) Time-mean circulation. (b) Standard deviation of the phase-shifted high-frequency eddies. (c) Tendency field induced by the heat flux of the phase-shifted high-frequency eddies. The contour interval for (a) and (b) is 0.2°C and 0.3°C, respectively; the contour interval for (c) is 0.05×10^{-5} °C s^{-1}. Only the relative geographical locations in this figure are dynamically meaningful but not the absolute geographical longitudes.

the wavenumbers 6 and 7 are the strongest high-frequency waves.

4. Baroclinic component of traveling storm tracks

Shown in Figs. 4–7 are the statistics of the phase-shifted temperature field at 700 mb following the low-frequency wavenumber $m_0 = 1$, 2, 3, and 4 of the 500-mb geopotential height at 50°N. It needs to be remembered that only the relative geographical locations on these maps are dynamically meaningful but not the absolute geographical longitudes. We have also calculated the statistics of the phase-shifted flow with the temperature and the geopotential height data from 850 mb to 200 mb. We have found that the maps shown in Figs. 5–8 in Part I are representative of the statistics of the phase-shifted geopotential height at all levels, whereas those shown in this section (i.e., Figs. 4–7 in

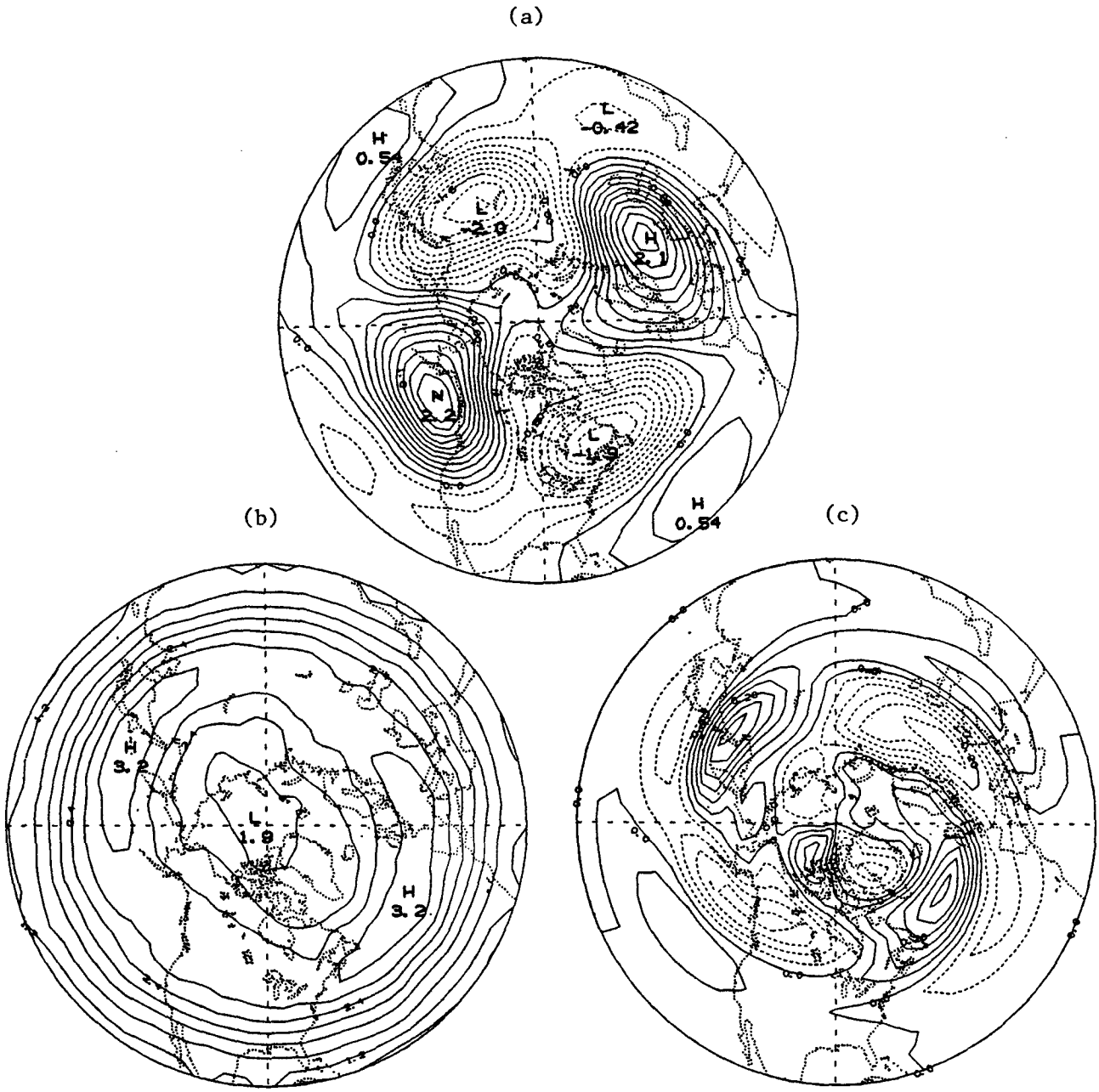

FIG. 5. As in Fig. 4 except for $m_0 = 2$.

this article) are representative of the statistics of the phase-shifted flow of the temperature field from 850 mb to 300 mb. The statistics at 200 mb shows some difference and will be addressed along with Figs. 12–13 later.

Panel (a) of Figs. 4–7 is the time-mean map of the phase-shifted low-frequency waves of the 700-mb temperature. It is seen that the time-mean temperature of the phase-shifted low-frequency waves primarily consists of the wavenumber m_0, where m_0 is the reference wavenumber we used to construct the phase-shifted flow. Hence, the phase-shifting technique is capable of filtering out all other waves not only at the reference level (the reference level is 500 mb) but also at all other levels, and not only in the reference variable (geopotential height) but also in temperature. The strength of our "filtering" approach will become clearer when we present the vertical structure of the phase-shifted low-frequency flows in next section. Apparently, a low-frequency wave has a deep vertical and robust

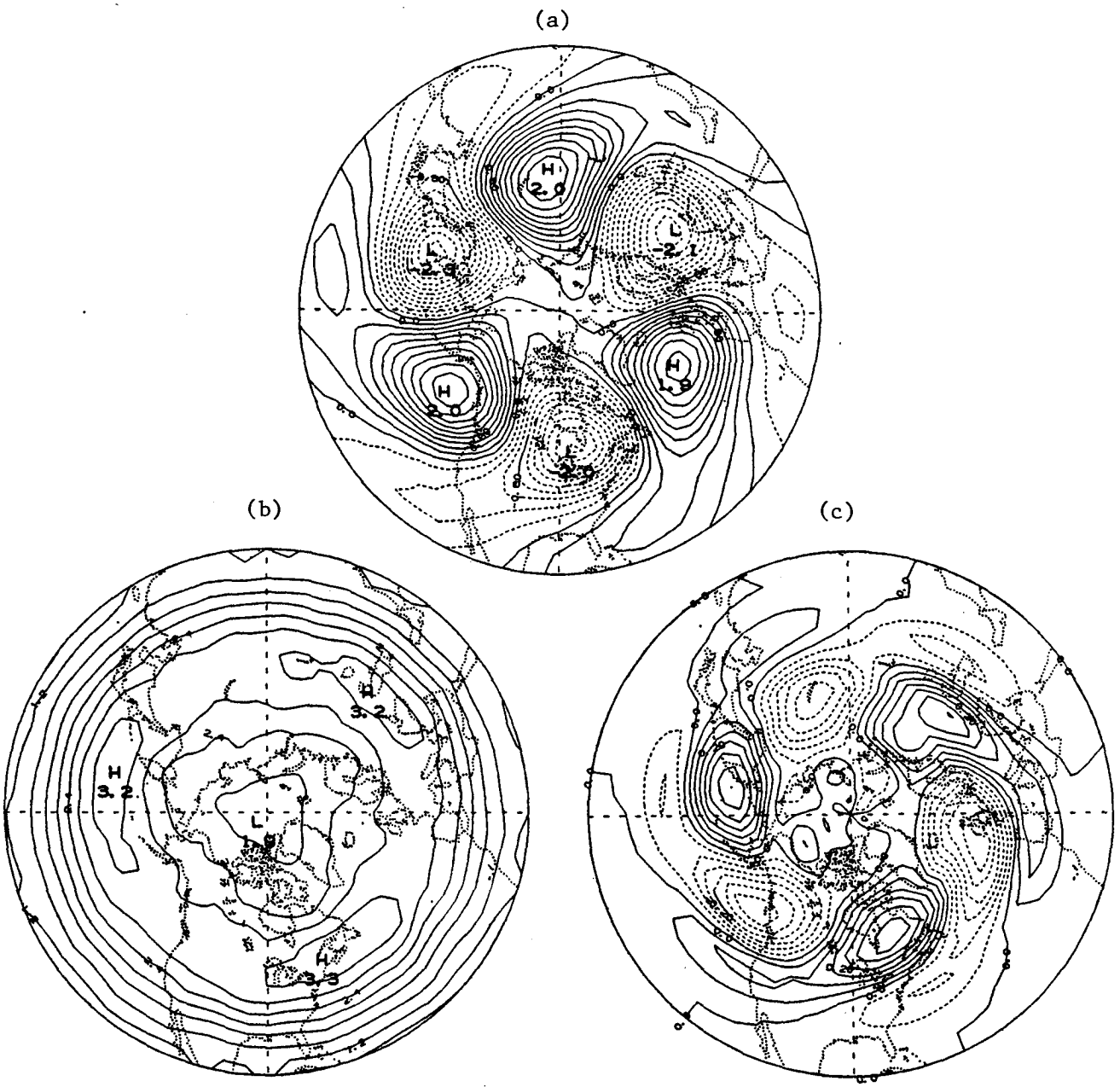

FIG. 6. As in Fig. 4 except for $m_0 = 3$.

meridional structure and travels with a more or less equal phase speed at all levels (otherwise we would lose the wave to be isolated at some levels far above or below the reference level).

The waves $m_0 = 1$, 2, 3, and 4 shown in panel (a) of Figs. 4–7 have nearly equal amplitude ($\approx$2.0°C) in midlatitude. According to Fig. 3b, the time-mean amplitude of the low-frequency waves of the 700-mb temperature is practically constant for $m_0 = 1$, 2, 3, and 4 ranging from 2.4°C to 2.2°C. Therefore, the phase-shifted low-frequency waves shown in panel (a) of these figures captures about 90% of the signal of the low-frequency waves of the 700-mb temperature. In other words, only 10% of the low-frequency wave m_0 of the 700-mb temperature is not coupled (or lined up consistently) with the low-frequency wave m_0 of the 500-mb geopotential height.

The rms maps of the phase-shifted high-frequency eddies of the 700-mb temperature with $m_0 = 1$, 2, 3, and 4 are shown in panel (b) of Figs. 4–7, respectively. The local maxima on each of the rms maps have a one-to-one correspondence with the troughs of the mean of the phase-shifted low-frequency flow shown in panel (a) of the same figure. For example, the rms

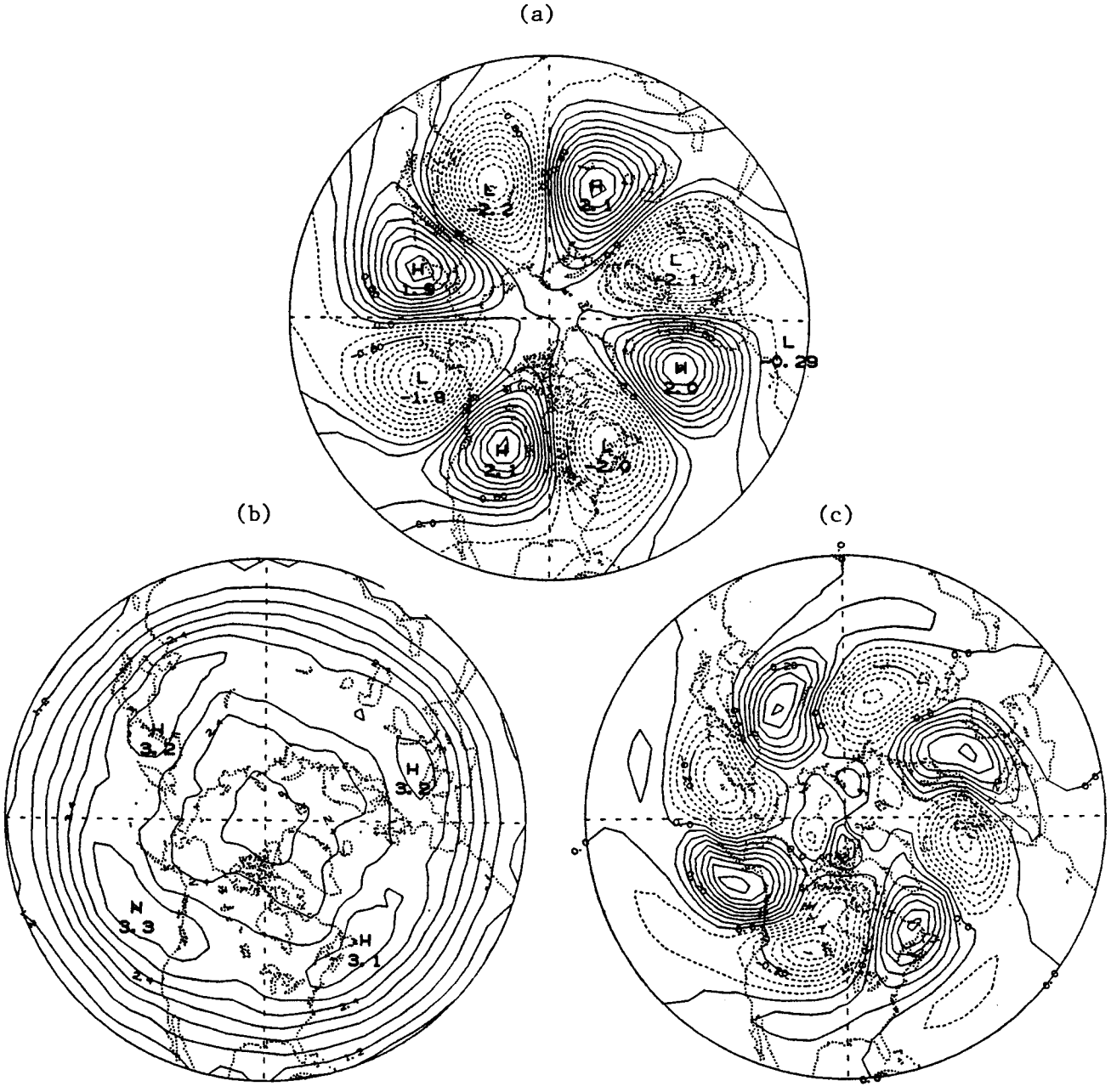

FIG. 7. As in Fig. 4 except for $m_0 = 4$.

map of the phase-shifted high-frequency eddies of the 700-mb temperature with $m_0 = 3$ exhibits three local maxima (Fig. 6b) downstream of the three troughs shown in Fig. 6a. These local maxima correspond to the traveling storm tracks. The intensity of the traveling storm tracks associated with each of the low-frequency planetary-scale waves is about the same (rms $\approx$ 3.2°C). The maximum rms of the non–phase-shifted high-frequency eddies (i.e., intensity of the stationary storm tracks) is about 4.5°C (not shown here). This, however, does not necessarily imply that the intensity of the traveling storm tracks is weaker than the stationary storm tracks since the traveling storm tracks shown in panel (b) of Figs. 4–7 are associated with only one low-frequency planetary-scale wave, whereas the stationary storm tracks are associated with the total stationary waves.

Panel (c) of Figs. 4–7 is the time-mean temperature feedback at 700 mb induced by the heat flux of the phase-shifted high-frequency eddies with $m_0 = 1, 2, 3,$

and 4. The dominant wave in the temperature tendency induced by the heat flux of the phase-shifted high-frequency eddies is identical to that in the mean of the phase-shifted low-frequency waves [panel (a) of the figures]. It is seen that the tendency maps shown in Figs. 4c and 5c also exhibit the alteration of the polarity in the meridional direction. The tendency maps shown in Figs. 6c and 7c are dominated with a monopole structure along the meridian. Most important, the temperature feedback of the traveling storm tracks in the mean is nearly out of phase with the low-frequency waves (m_0 = 1, 2, 3, and 4). This suggests that the traveling storm tracks act to diminish the baroclinic component of the low-frequency waves. At a rate of -0.3°C per day, the high-frequency eddies would, if unopposed, erode the low-frequency waves in T(2°C) in a week.

We have also obtained the time-mean maps of the phase-shifted low-frequency component of the temperature tendency χ^T calculated directly from the original (i.e., non–phase-shifted) high-frequency transients. These maps are found to be nearly identical to those shown in panel (c) of Figs. 4–7 (the counterpart results for χ^Z were reported in Part I). This implies that the waves in panel (c) of Figs. 4–7 are not associated with the climatological stationary feedbacks induced by the high-frequency eddies since the low-frequency component of the feedbacks by definition is free from the climatological mean.

5. Vertical structure of low-frequency waves and feedbacks

We have constructed the phase-shifted low-frequency waves at each level by following the low-frequency wave m_0 (m_0 = 1, 2, 3, 4) of the 500-mb geopotential height at 50°N. We may then determine the vertical structure of the time mean of the phase-shifted low-frequency waves as well as the vertical structure of the feedbacks on the low-frequency waves induced by the high-frequency eddies. Figures 8–11 are the vertical cross-section diagrams for the mean circulation along the latitude 50°N deduced from the moving frame following the low-frequency wave m_0 of the 500-mb geopotential height at 50°N with m_0 = 1, 2, 3, 4, respectively. Panels (a) and (b) of these figures are the mean geopotential height and temperature of the phase-shifted low-frequency waves. Panels (c) and (d) are

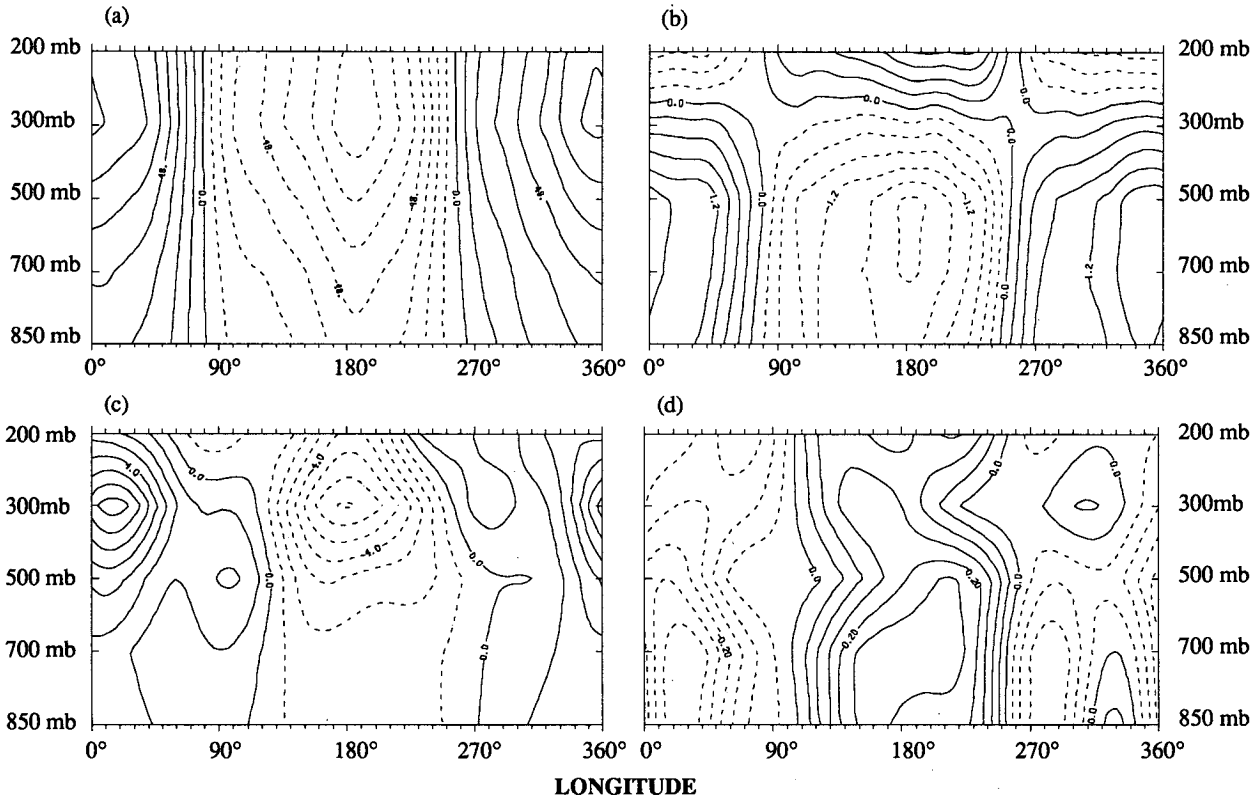

FIG. 8. Vertical cross-section diagram of the mean circulation recorded in the moving frame that follows the low-frequency wave m_0 = 1 of the 500-mb geopotential height at 50°N. (a) Geopotential height; (b) temperature; (c) the geopotential height tendency induced by the vorticity flux of the high-frequency eddies. (d) The temperature tendency induced by the heat flux of the high-frequency eddies. The contour intervals for panels (a)–(d) are 12 m, 0.3°C, 1.0×10^{-5} m s^{-1}, and 0.05×10^{-5} °C s^{-1}, respectively. Only the relative geographical locations in this figure are dynamically meaningful but not the absolute geographical longitudes.

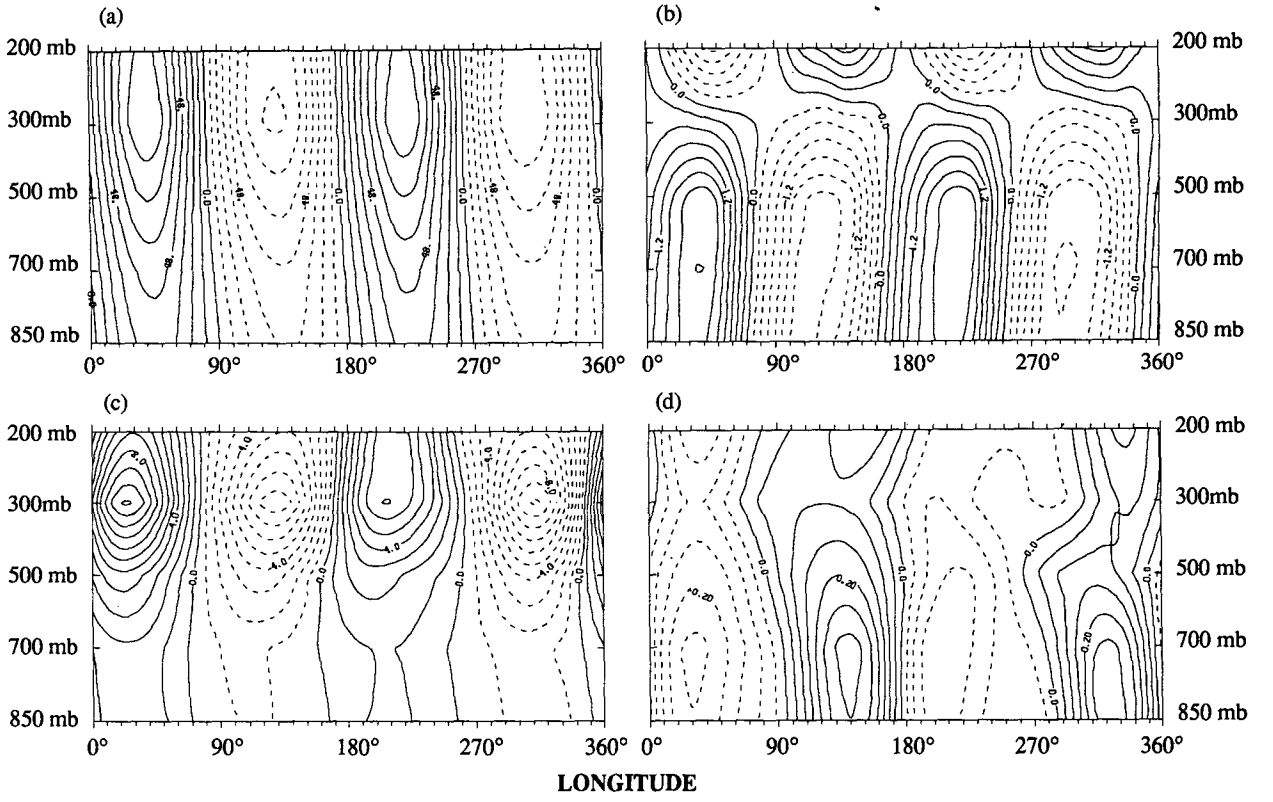

FIG. 9. As in Fig. 8 except for $m_0 = 2$.

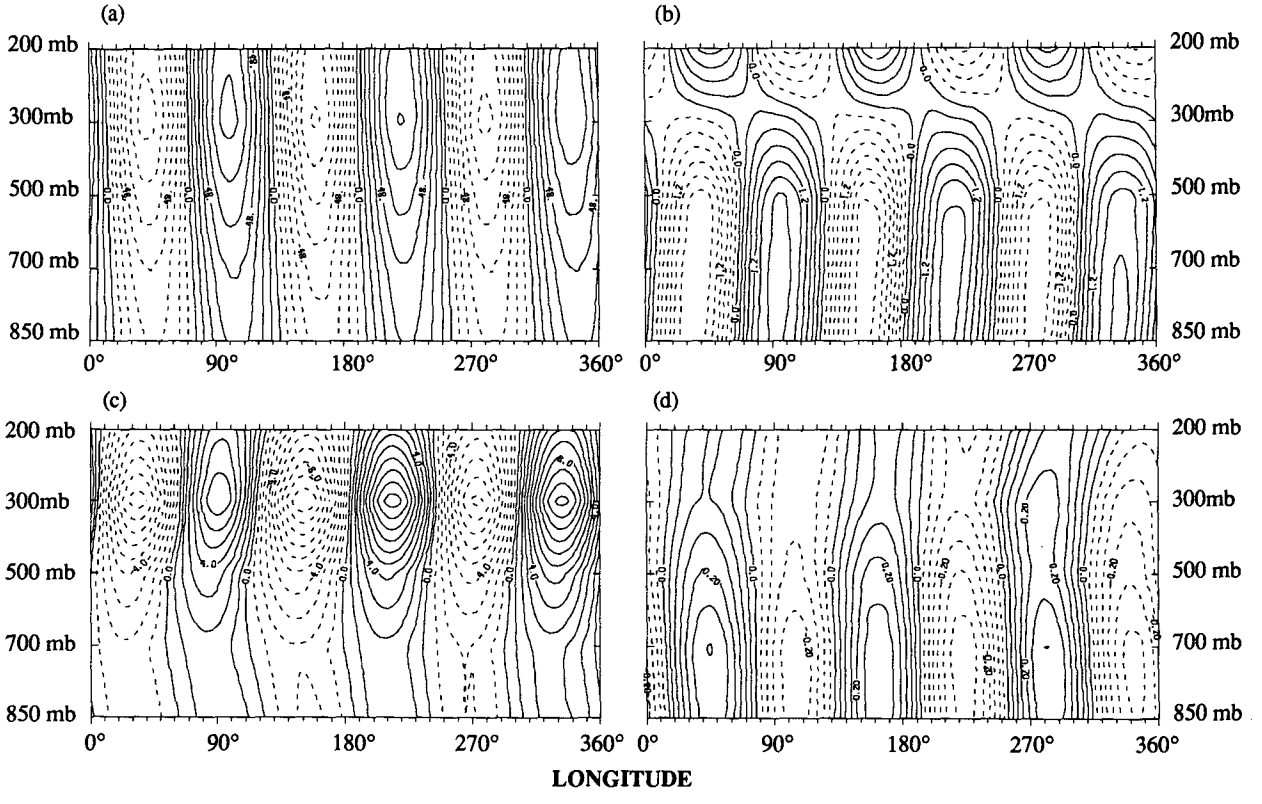

FIG. 10. As in Fig. 8 except for $m_0 = 3$.

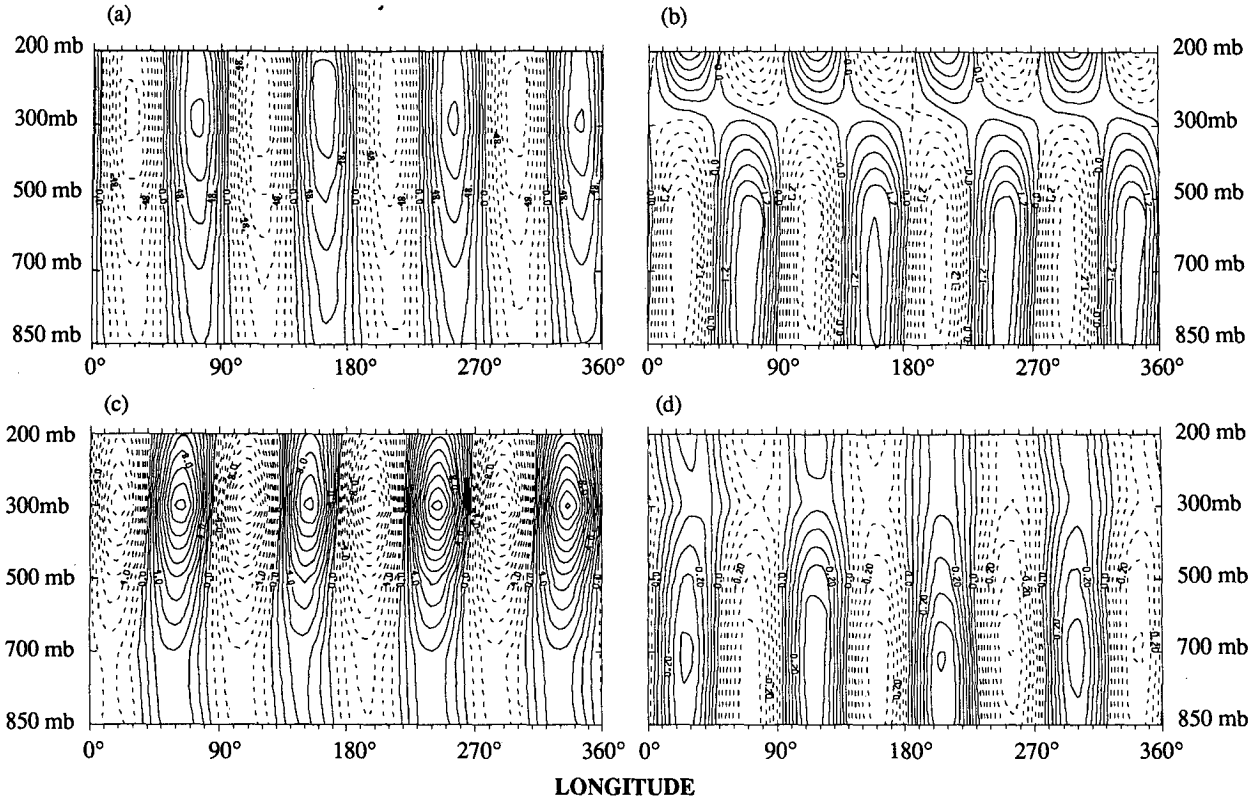

FIG. 11. As in Fig. 8 except for $m_0 = 4$.

the mean barotropic and baroclinic feedbacks of the high-frequency eddies on the low-frequency waves. All four panels shown in each of the figures are obtained in the same moving frame. Hence, there no ambiguity in interpreting the vertical structure of the phase-shifted low-frequency waves and its relationship with low-frequency temperature field and the feedbacks due to the high frequency.

One of the very striking features shown in panel (a) of these figures is the equivalent barotropic structure of the low-frequency waves. This is rather different from stationary waves (cf. Fig. 1a). The amplitude of the low-frequency waves reaches its maximum value at 300 mb, consistent with the results shown in Fig. 2b. Moreover, the amplitude of the waves as well its vertical variation shown in panel (a) of these figures is nearly equal to that shown in Fig. 2b, indicating that the low-frequency waves at all levels travel with more or less the same speed in the mean.

Panel (b) of these figures is the counterpart of panel (a) for the phase-shifted low-frequency waves in temperature. Again there is very little vertical tilt of the mean temperature of the low-frequency waves. The change in polarity of the low-frequency waves in T near 250 mb is very likely a manifestation of the tropopause. The maximum amplitude of the phase-shifted low-frequency waves in T is at 700 mb. According to Fig. 3b, the low-frequency waves of the temperature actually are strongest at 850 mb. This suggests that the mean phase speed of a low-frequency wave in T at lower levels is slightly different from that of the same low-frequency wave in the 500-mb geopotential height with subsequent loss of amplitude in the composing process. Nevertheless, the difference is very small so that phase-shifting technique captures most of the signal of the low-frequency waves in T. The nearly in-phase relation between the waves shown in panel (a) and those in panel (b) is supplementary evidence that the time-mean structure of the low-frequency waves is equivalent barotropic. Note also that panels (a) and (b) are in visual hydrostatic agreement.

Panel (c) of these figures shows the vertical cross-section diagram of the geopotential height tendency induced by the vorticity flux of the phase-shifted high-frequency eddies. This figure should be compared to panel (a) to examine the relation between the low-frequency waves and the traveling storm tracks. The general feature is that the vorticity flux associated with the traveling storm tracks acts to reinforce the low-frequency waves throughout the troposphere. The maximum of the positive barotropic feedback takes place at 300 mb, where the amplitude of the low-frequency waves of the geopotential height is the largest. It is of interest to point out that the positive barotropic

feedback on a low-frequency wave with a shorter wavelength is slightly stronger than that on a longer wave. The positive feedback of the high-frequency eddies on the stationary waves, however, exhibits the maximum strength at the wavenumbers 1 and 3 and the feedbacks upon the wavenumbers 2 and 4 are considerably weaker (not shown here). Panel (d) is the temperature tendency induced by the heat flux of the phase-shifted high-frequency eddies. Comparing panel (d) with panel (b) indicates that the temperature feedback of the high-frequency eddies is nearly out of phase with the low-frequency waves in T throughout the column except for the region above 300 mb, where the temperature feedback is nearly in phase with the low-frequency waves. The strongest negative temperature feedback occurs at 700 mb.

The relation between the low-frequency waves and the high-frequency eddies at 200 mb needs to be examined in further detail since at this level, both the barotropic and baroclinic feedbacks act to reinforce the low-frequency waves. Shown in Figs. 12 and 13 are the statistics of the phase-shifted geopotential height and temperature data at 200 mb with $m_0 = 3$. The mean of the phase-shifted low-frequency flow [panel (a) of these two figures] is again dominated by the wavenumber 3 in the zonal direction. The traveling storm tracks are identifiable in both the geopotential height and temperature fields [panel (b) of these two figures]. It is important to note that the traveling storm tracks at 200 mb are located over the trough regions of the low-frequency waves of the geopotential height, but over the ridge regions of the temperature. The tendency maps [panel (c) of these two figures] clearly suggest that both the barotropic and baroclinic feedbacks act to reinforce the low-frequency waves over the whole plane. The statistics of the phase-shifted flow at 200 mb with other values of m_0 reveal a similar spatially coherent relation between the low-frequency waves and the high-frequency eddies. Interestingly, the stationary storm tracks at 200 mb are also located over the trough regions of the stationary waves of the geopotential height but over the ridge regions of the temperature (not shown here). The feedbacks of the high-frequency eddies associated with the stationary storm tracks at 200 mb tend to reinforce the stationary waves both barotropically and baroclinically.

6. Summary and discussion

In this two-part study, we have presented the spatially coherent relation between the low-frequency waves and the high-frequency eddies using a ten-year winter dataset of the geopotential height and temperature over the Northern Hemisphere. Our main findings are: 1) The amplitude of the planetary-scale low-frequency waves is nearly constant with zonal wavenumber and has a maximum at 300 mb for geopotential height and at 850 mb for temperature; 2) All low-frequency waves have a nearly equivalent barotropic structure; 3) The instantaneous zonal phase speed of an individual low-frequency wave is nearly independent of height so that we may identify the three-dimensional structure of a low-frequency wave by following the same wave at just one pressure level; 4) The traveling storm tracks, defined as the local maxima on the rms map of the phase-shifted high-frequency eddies, are located over the trough regions of the low-frequency waves; 5) The barotropic feedback of the traveling storm tracks tends to reinforce the low-frequency waves of the geopotential height throughout the troposphere; 6) The baroclinic feedback of the traveling storm tracks appears to have an out-of-phase relation with the low-frequency waves of the temperature from 850 mb to 300 mb. At 200 mb, the baroclinic feedback is nearly in phase with the low-frequency waves of the temperature.

We now discuss the implications of our study on four theoretical issues concerning the dynamics of the midlatitude general circulation.

a. The net total effect of eddies on mean flow

A question often asked is about the *net* effect of the high-frequency transients on the mean flow (the low-frequency flow in our case). In Figs. 1 and 8–11, we purposely displayed χ^Z and χ^T separately. Under a few assumptions (which may or may not be valid) χ^Z and χ^T can be combined into a single term as the net one-time-step tendency induced by the high-frequency eddies. Here we give two ways of doing this and then proceed to discuss the validity of these approaches.

(i) The height tendency due to the heat flux of the transients can be determined from χ^T through the hydrostatic relation. The sum of the height tendencies due to vorticity and heat fluxes then measures the total height tendency of the transients. Alternatively, the temperature tendency due to the vorticity flux of the transients is proportional to the derivative of χ^Z with respect to p (assuming hydrostatic balance) and then the sum of the temperature tendency due to the vorticity and heat fluxes gives rise to the total temperature tendency of the transients. We suspect many readers have done this by eye when seeing panels (c) and (d) in Fig. 1 and Figs. 8–11. In doing so, one can note a fair amount of compensation in $\partial Z/\partial t$ due to the vorticity and heat fluxes of the high-frequency transients in the upper levels, which is in agreement with the findings of Lau and Holopainen (1984) and Lau and Nath (1991). The compensation in $\partial T/\partial t$ due to the vorticity and heat fluxes of the high-frequency transients, on the other hand, mainly takes place at the lower levels. It should be noted again that the effect of so-called secondary circulation is not included in both χ^Z and χ^T.

(ii) A slightly more elaborate way is to solve the quasigeostrophic potential vorticity equation (e.g., Lau and Holopainen 1984)

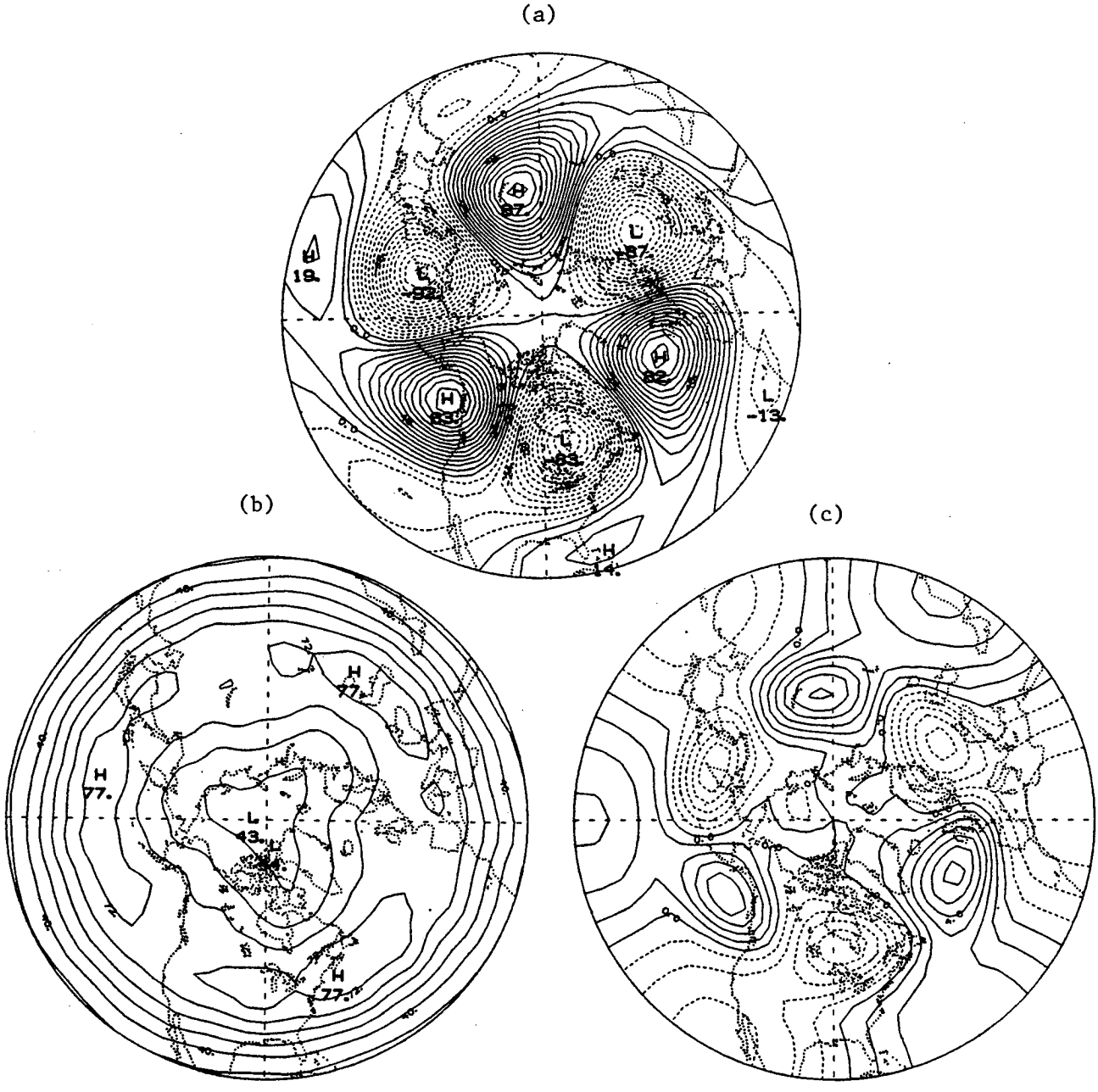

FIG. 12. Statistics of the phase-shifted flow of the 200-mb geopotential height with $m_0 = 3$. (a) Time-mean circulation. (b) Standard deviation of the phase-shifted high-frequency eddies. (c) Tendency field induced by the vorticity flux of the phase-shifted high-frequency eddies. The contour interval for (a) and (b) is 6.0 m and that for (c) is 1.0×10^{-5} m s^{-1}. Only the relative geographical locations in this figure are dynamically meaningful but not the absolute geographical longitudes.

$$\left\{\nabla^2 + f_0^2 \frac{\partial}{\partial p}\left(\frac{1}{\sigma}\frac{\partial}{\partial p}\right)\right\}\frac{\partial \Phi}{\partial t} = -f_0 \nabla \cdot (\mathbf{v}'\zeta') - f_0^2 R \frac{\partial}{\partial p}\left(\frac{\nabla \cdot (\mathbf{v}'T')}{-\sigma p}\right) + \text{other terms}, \quad (3)$$

with boundary conditions. Again the terms with prime are derived from the high-frequency eddies. In this method, in addition to the terms defined in (1a) and (1b), the net total effect of the eddies now also includes the impact of the secondary circulation, which is required to maintain the hydrostatic and geostrophic balances. It has been found previously that the correction due to the secondary circulation is generally small (e.g., Pfeffer 1981; Lau and Holopainen 1984; Pierrehumbert 1986; Lau and Nath 1991) and so one can reduce (3) to the separable (1a) and (1b) without losing too much accuracy.

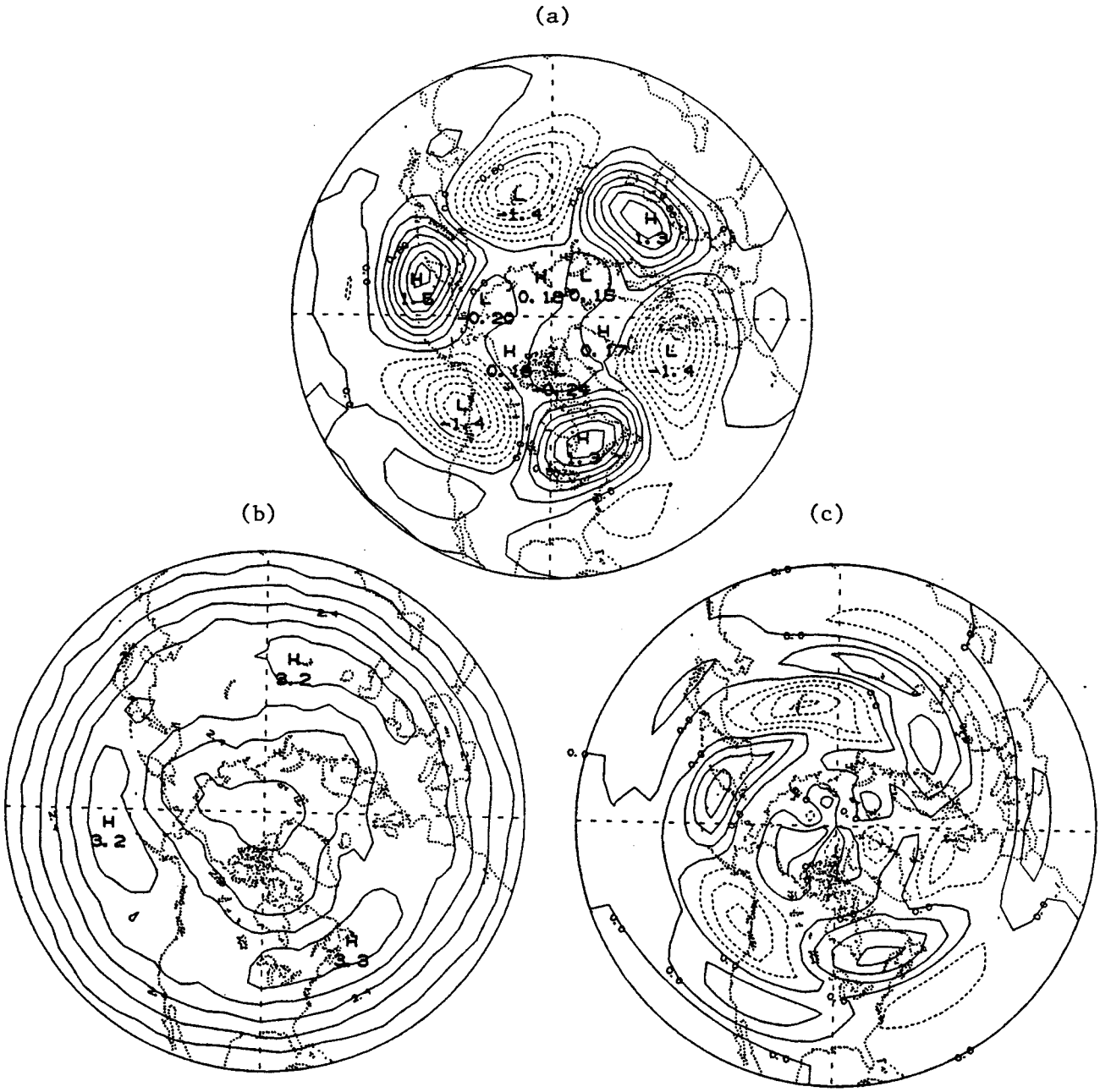

FIG. 13. As in Fig. 12 except for temperature. The contour interval for (a) and (b) is 0.2°C and 0.3°C, respectively; the contour interval for (c) is 0.05×10^{-5} °C s^{-1}.

Given that (3) has a lot more terms on the right-hand side, one can call into question the assumption that the net effect of the eddies themselves should be quasigeostrophic and hydrostatic [recall that Eq. (3) is solved with the two transients terms only in assessing the feedback effect of the transients]. This assumption is reasonable if the two eddy terms are the largest (as is the case in the zonally averaged framework). If, however, the horizontal eddy fluxes are counterbalanced by other horizontal fluxes (involving the mean flow, for instance), the need for vertical circulation required to maintain the quasigeostrophic and hydrostatic balances would change completely. Another fundamental problem is that while upper and lower boundary conditions are known for the total flow, there is no obvious vertical boundary conditions for part of the total tendencies.

Given these problems, we view that there is lack of scientific basis for one to "add" panels (c) and (d) in Figs. 1 and 8–11, and so we leave them separately

without formally evaluating the *net* total effect of the high-frequency transients on the low-frequency flow.

b. *Local instability theory*

The theoretical work of Frederiksen (1983), Pierrehumbert (1984), and Cai and Mak (1990a) has suggested that the phenomenon of the frequent cyclogenesis over the downstream regions of the major troughs of the stationary waves can be viewed as a manifestation of the local instability of a zonally varying atmospheric flow. This is to be contrasted to the classic-intuitive view that the existence of the (stationary) storm tracks is a direct consequence of the geographically fixed, zonally asymmetric boundary forcings such as the ocean–land contrast and mountains. The main characteristics of the spatially coherent relation between a zonally asymmetric basic flow and the localized disturbances are (i) the amplitude of a local mode reaches its maximum at a distance somewhat downstream of the point of the maximum baroclinicity of the basic flow; (ii) the vorticity flux induced by the localized disturbance tends to reinforce the barotropic component of the basic flow; (iii) the heat flux of the disturbance, on the other hand, acts to diminish the baroclinic component of the basic flow [see Fig. 9 in Cai and Mak (1990a) for evidence of items (ii) and (iii)]. The close resemblance between the theoretical prediction and the observations (e.g., Blackmon et al. 1977; Lau and Holopainen 1984), together with the fact that the baroclinically unstable local modes typically have a time scale of a few days and a spatial scale of several thousand kilometers, makes the local instability theory an appealing candidate to explain the existence of the (stationary) storm tracks downstream of the climatological jet streams. Recall that the main assumption made in a typical local instability analysis is the *independence* of the disturbance on the geographically fixed, zonally asymmetric boundary forcings that maintain the basic flow. This assumption enables us to explain the localized disturbances solely in terms of the zonal inhomogeneity of the basic flow. Our present observational study seems to validate the assumption further by showing the existence of traveling storm tracks associated with the traveling planetary-scale waves (if we were to fail to identify the traveling storm tracks, we would have to conclude that the zonal inhomogeneity in the traveling low-frequency waves was dynamically different from that in the stationary waves in order to believe the local instability theory). Moreover, the disturbances associated with the traveling storm tracks also appear to have the same dual-feedback effect on the barotropic and baroclinic components of the traveling planetary-scale waves. Therefore, our observational study appears to support the local instability theory that accounts for the existence of the stationary/traveling storm tracks as the consequence of the zonal inhomogeneity of the climatological mean/low-frequency flow rather than as the direct consequence of the asymmetric lower boundary conditions such as land–ocean contrast and large-scale topography. Nevertheless, the zonal inhomogeneity of the climatological mean flow is still related to the zonally asymmetric lower boundary conditions. It is known that the zonal asymmetry in the lower boundary conditions in the Southern Hemisphere is much weaker than that in the Northern Hemisphere. As a result, the climatological mean flow over the Southern Hemisphere has less zonal asymmetry than its counterpart over the Northern Hemisphere. However, there is no lack of variability in either low- or high-frequency transients over the Southern Hemisphere except that the variability appears to be more zonally uniform (Trenberth 1981, 1991). It is expected that the symbiotic relation between the low- and high-frequency transients found in this study would play an even more significant role in the Southern Hemisphere.

While we have presented strong evidence that the theory of local instability explains the dynamics of stationary storm tracks, we also point out that this does not invalidate other mechanisms. For example, the Gulf Stream and the land–ocean contrast obviously play an important role in determining the path and intensity of an individual cyclone over the U.S. east coast.

c. *Low-frequency variability of the midlatitude circulation*

Unlike the stationary waves, the low-frequency waves are characterized by a rather flat spectrum in the range of zonal wavenumber 1–4 throughout the whole column of the atmosphere (cf. Figs. 2 and 3). Coincidently or not, the feedbacks of the high-frequency eddies also exhibit a relatively uniform distribution among the waves 1–4 (Figs. 10 and 11). Another important feature of the midlatitude low-frequency waves is that the phase speeds at different latitudes and pressure levels are more or less the same so that we may detect the three-dimensional structure of a low-frequency wave by following the phase speed of the same wave at a particular latitude and pressure level in either Z or T.

The dual-feedback effect of the high-frequency eddies on the low-frequency waves seems to complicate the notion of the forcing mechanism of low-frequency waves by high-frequency eddies. From an energetics point of view, the positive (or in-phase) feedback of the high-frequency eddies upon the barotropic component of the low-frequency waves implies a net kinetic energy conversion from the high-frequency eddies to the low-frequency waves. Likewise, the negative (or out-of-phase) feedback of the high-frequency eddies upon the baroclinic component of the low-frequency waves means a net potential energy conversion from the low-frequency waves to the high-frequency eddies.

The interpretation of the feedback effects from the energetics point view is consistent with earlier findings of Kung and Tanaka (1983), Holopainen and Fortelius (1987), and Sheng and Hayashi (1991), which shows downscale energy transfer of available potential energy and upscale energy transfer of kinetic energy for the midlatitude atmospheric circulation.

It is, however, still plausible that the high-frequency eddies in the mean act as an energy source to the low-frequency waves. We may speculate the mechanism for the interaction between the low-frequency waves and the high-frequency eddies as follows. The zonal inhomogeneity of low-frequency waves alternates the background baroclinicity in which the high-frequency eddies are embedded. As a result, the high-frequency eddies tend to develop preferentially over the trough region of the low-frequency waves through local baroclinic instability. The development of the high-frequency eddies would result in a negative baroclinic feedback by transporting the heat downgradient of the background baroclinicity. The positive barotropic feedback is essential for the low-frequency waves being able to continuously organize the high-frequency eddies. The ultimate energy source for the high-frequency eddies is still the zonal potential energy created by the differential heating across the latitudes. What the low-frequency waves do is to make the release of the zonal potential energy more probable over certain regions (i.e., troughs) than other regions. This implies that the low-frequency waves would effectively lose part of their potential energy to the high-frequency eddies. But the low-frequency waves have a net energy return from the high-frequency eddies through the upscale energy cascade (a barotropic process). The symbiotic relation between low- and high-frequency transients hypothesized in the foregoing is supported by the numerical results of Cai and Mak (1990b) and Robinson (1991) derived from a two-layer model. We plan to perform an energetics analysis in a future study to clarify the issue of the importance of the barotropic forcing versus the baroclinic damping during the life cycles of the low-frequency waves.

d. Critique

It has become customary to study the coupling of low-frequency variability and high-frequency eddies by examining the spatially coherent relation between the low-frequency waves and tendencies (or feedbacks) induced by the high-frequency eddies. It is important to note that the resemblance between, for instance, the barotropic feedback and the low-frequency flow does not, in itself, mean that the low-frequency flow is the response to the tendency induced by vorticity flux of the high-frequency eddies. The evolution of low-frequency waves is actually determined by many internal interactive chains and the external forcings. Those internal interactive chains include (i) the linear interaction between the time-mean flow and low-frequency waves, (ii) nonlinear interactions among the low-frequency waves as well as between low- and high-frequency transients, and (iii) the interaction among the high-frequency eddies (i.e., the feedbacks of high-frequency eddies). The high-frequency transient eddy forcing could only be a minor contribution to the total observed tendency of the low-frequency waves. Hence, it is important to document the relation between the observed tendency of the low-frequency waves and the tendencies induced by various processes. We expect that some of the internal interactive chains are related more to the observed tendency ($\partial Z/\partial t$) than to the low-frequency waves (Z) themselves. Obviously, these internal processes would primarily account for propagation of the low-frequency waves and play little role in terms of providing energy to the low-frequency waves. However, the processes that contribute little to the observed tendency but have good spatial correlation with the low-frequency waves themselves may act to "maintain/damp" the low-frequency waves by providing/drawing energy to/from low-frequency waves because the energy generation term is proportional to $Z\chi^Z$ instead of $(\partial Z/\partial t)\chi^Z$, where χ^Z is the tendency evaluated from a term on the left-hand side of the vorticity equation. The key appears to be the energy consideration, or alternatively, the distinction between time tendencies due to propagation on the one hand and amplitude growth or decay on the other. Following a wave eliminates, in a sense, propagation. Details of analyses along this line will be the subject of a future study.

Acknowledgments. This research was supported by NOAA under Grant NA89-AA-H-MC066 and National Science Foundation under Grant ATM-9103647. The helpful criticism and suggestions from the two reviewers have led to significant improvement of the presentation and are much appreciated.

REFERENCES

Blackmon, M. L., 1976: A climatological spectral study of the 500 mb geopotential height of the Northern Hemisphere. *J. Atmos. Sci.*, **33**, 1607–1623.

——, J. M. Wallace, N. C. Lau, and S. L. Mullen, 1977: An observational study of Northern Hemisphere wintertime circulation. *J. Atmos. Sci.*, **34**, 1040–1053.

Cai, M., and M. Mak, 1990a: On the basic dynamics of regional cyclogenesis. *J. Atmos. Sci.*, **47**, 1417–1442.

——, and ——, 1990b: Symbiotic relation between planetary and synoptic scale waves. *J. Atmos. Sci.*, **47**, 2953–2968.

——, and H. M. van den Dool, 1991: Low-frequency waves and traveling storm tracks. Part I: Barotropic component. *J. Atmos. Sci.*, **48**, 1420–1436.

Frederiksen, J. S., 1983: Disturbances and eddy fluxes in Northern Hemisphere flows: Instability of three-dimensional January and July flows. *J. Atmos. Sci.*, **40**, 836–855.

Holopainen, E., and C. Fortelius, 1987: High-frequency transient eddies and blocking. *J. Atmos. Sci.*, **44**, 1632–1645.

Hoskins, B. J., I. N. James, and G. H. White, 1983: The shape, propagation and mean-flow interaction of large-scale weather systems. *J. Atmos. Sci.*, **40**, 1595–1612.

Kung, E. C., and H. Tanaka, 1983: Energetics analysis of the global circulation during the special observation periods of FGGE. *J. Atmos. Sci.*, **40,** 2575–2592.

Lau, N. C., 1988: Variability of the observed midlatitude storm tracks in relation to low frequency changes in the circulation pattern. *J. Atmos. Sci.*, **45,** 2718–2743.

——, and E. O. Holopainen, 1984: Transient eddy forcing of the time-mean flow as identified by geopotential tendencies. *J. Atmos. Sci.*, **41,** 313–328.

——, and J. Nath, 1991: Variability of the baroclinic and barotropic transient eddy forcing associated with monthly changes in the midlatitude storm tracks. *J. Atmos. Sci.*, **48,** 2589–2613.

Metz, W., 1989: Low-frequency anomalies of atmospheric flow and the effects of cyclone-scale eddies: A canonical correlation analysis. *J. Atmos. Sci.*, **46,** 1026–1041.

——, 1990: Empirical modeling of extratropical cyclone vorticity fluxes. *Tellus,* **42A,** 14–27.

——, 1991: Optimal relationship of large-scale flow patterns and the barotropic feedback due to high-frequency eddies. *J. Atmos. Sci.*, **48,** 1141–1159.

Pfeffer, R. L., 1981: Wave–mean-flow interactions in the atmosphere. *J. Atmos. Sci.*, **38,** 1340–1359.

Pierrehumbert, R. T., 1984: Local and global baroclinic instability of zonally varying flow. *J. Atmos. Sci.*, **41,** 2141–2162.

——, 1986: The effect of local baroclinic instability of zonally varying flow. *Adv. Geophys.*, **29,** 165–182.

Robinson, W., 1991: The dynamics of low-frequency variability in a simple model of the global atmosphere. *J. Atmos. Sci.*, **48,** 429–441.

Sheng, J., and Y. Hayashi, 1990: Estimation of atmospheric energetics in the frequency domain during the FGGE year. *J. Atmos. Sci.*, **47,** 1255–1268.

Trenberth, K. E., 1981: Observed Southern Hemisphere eddy statistics at 500 mb: Frequency and spatial dependence. *J. Atmos. Sci.*, **38,** 2585–2605.

——, 1991: Storm tracks in the Southern Hemisphere. *J. Atmos. Sci.*, **48,** 2159–2178.

Wallace, J. M., 1983: The climatological mean stationary waves: Observational evidence. *Large-Scale Dynamical Processes in the Atmosphere.* 27–54. B. J. Hoskins and R. P. Pearce, Eds. Academic Press. 397 pp.

——, and M. L. Blackmon, 1983: Observations of low-frequency atmospheric variability. *Large-Scale Dynamical Processes in the Atmosphere.* B. J. Hoskins and R. P. Pearce, Eds. Academic Press. 397 pp.